Pergamon

0956-7151(94)E0136-5

Acta metall. mater. Vol. 42, No. 10, pp. 3451–3461, 1994

0956-7151/94 $7.00 + 0.00

ON THE TENSILE PROPERTIES OF A FIBER REINFORCED TITANIUM MATRIX COMPOSITE—II. INFLUENCE OF NOTCHES AND HOLES

S. J. CONNELL, F. W. ZOK, Z. Z. DU and Z. SUO

Departments of Materials and Mechanical and Environmental Engineering, University of California, Santa Barbara, CA 93106, U.S.A.

(Received 19 January 1994)

Abstract—The effects of holes and notches on the ultimate tensile strength of a unidirectionally reinforced titanium matrix composite have been examined. During tensile loading, a narrow plastic strip forms ahead of the notch or hole prior to fracture, similar to that observed in thin sheets of ductile metals. Examination of the fibers following dissolution of the matrix indicates that essentially all the fibers within such a strip are broken prior to catastrophic fracture of the composite. The trends in notch-strength have been rationalized using a fracture mechanics-based model, treating the plastic strip as a bridged crack. The observations suggest that the bridging traction law appropriate to this class of composite is comprised of two parts. In the first, the majority of fibers are unbroken and the bridging stress corresponds to the unnotched tensile strength of the composite; in the second, the fibers are broken and the bridging stress is governed by the yield stress of the matrix, with some contribution derived from fiber pullout. This behavior has been modeled by a two-level rectilinear bridging law. The parameters characterizing the bridging law have been measured and used to predict the notch strength of the composite. A variation on this scheme in which the fracture resistance is characterized by an intrinsic toughness in combination with a rectilinear bridging traction law has also been considered and found to be consistent with the predictions based on the two-level traction law.

1. INTRODUCTION

Fiber-reinforced titanium matrix composites are being considered for structural applications in advanced aerospace engines [1]. It is envisioned that, in some applications, holes will be introduced for either fastening or cooling. The design of such structures will require an understanding of the damage processes occurring around the holes and the influence of damage on structural performance. The intent of the present article is to examine the nature of such processes and to assess the utility of non-linear fracture mechanics-based models for describing the influence of holes and notches on tensile strength.

It will become evident that the trends in strength with hole or notch size can be rationalized in terms of models based on crack bridging, analogous to those used to describe the notch sensitivity of monolithic ductile metals and ceramic matrix composites (CMCs). As a result, the following section provides a brief review of the existing crack bridging models. The review is followed by a description of the experimental portion of the study and comparisons with the model predictions.

†Corresponding to either plane stress or plane strain conditions, as appropriate.

‡Neglecting the effects of volume on strength.

2. BACKGROUND ON NOTCH SENSITIVITY

In brittle materials, the tensile strength $\bar{\sigma}$ of a panel containing a sharp, through-thickness *notch* can be described by the Griffith equation

$$\bar{\sigma} = \sqrt{\frac{E\Gamma}{\pi a_0}} \tag{1}$$

where Γ is the toughness, E is Young's modulus† and $2a_0$ is the notch length. Alternatively, if the panel contains a circular hole with a radius a_0 that is large in comparison to the intrinsic flaw size, c, the strength is given by

$$\bar{\sigma} = \frac{1}{3}\sqrt{\frac{E\Gamma}{\pi c}}. \tag{2}$$

In essence, the hole reduces the strength by a factor equivalent to the stress concentration factor ($k_t = 3$), independent of the absolute hole size‡. Consequently, equation (2) can be re-written as

$$\bar{\sigma} = \bar{\sigma}_0/3 \tag{3}$$

where $\bar{\sigma}_0$ is the tensile strength in the absence of a hole or a notch.

Ductile materials, particularly in the form of thin sheet, behave differently. In the presence of a notch, tensile fracture is preceded by the development of a narrow zone of intense plasticity ahead of the notch [2]. Fracture occurs by the formation and propagation of a crack within the plastic zone. This process

can be modeled by considering the tip of the plastic zone to be the tip of a hypothetical crack and the material within the plastic strip to be a "bridged zone" [3, 4]. The tractions exerted by the bridged zone are taken to be equivalent to the yield stress of the metal, σ_y. Moreover, the intrinsic fracture energy, Γ_0, is taken to be zero, such that all the fracture resistance is derived from bridging. Using the J-integral, the contribution derived from bridging, Γ_b, can be expressed as [5]

$$\Gamma_b = \int_0^{\delta_c} \sigma_y \, d\,\delta = \sigma_y \delta_c \tag{4}$$

where δ is the crack opening displacement and δ_c is the critical value needed to fracture the metal. Moreover, the fracture stress varies with notch size according to the relation [4]

$$\frac{\bar{\sigma}}{\bar{\sigma}_0} = \frac{2}{\pi} \cos^{-1}\left(\exp \frac{-\pi}{8\alpha}\right) \tag{5a}$$

where α is a normalized measure of the notch size

$$\alpha \equiv \frac{a_0 \bar{\sigma}_0^2}{\Gamma E} \tag{5b}$$

and the unnotched tensile strength, $\bar{\sigma}_0$, is taken to be the yield stress, σ_y. This approach is commonly referred to as the Dugdale–Barenblatt model.

The parameter used to normalize the notch size, $\Gamma E/\bar{\sigma}_0^2$, is a characteristic bridging length scale that governs the degree of notch sensitivity. When this length scale is large compared to the notch length, the tensile strength is reached after the plastic strip extends only a small amount and thus the steady-state toughness, given by equation (4), is not fully realized. Conversely, when the bridging length scale is sufficiently small, the toughness is fully utilized prior to catastrophic fracture, whereupon the stress-notch length relation [equation (5)] reduces to the Griffith relation [equation (1)].

More recently, models based on crack bridging have been developed for predicting the notch-strength characteristics of ceramic matrix composites (CMCs) [6–8]. The essential difference between these models and the one developed by Dugdale involves the functional form of the bridging traction law. The traction laws considered to date include linear softening, linear hardening and parabolic hardening, in addition to the rectilinear law. Figure 1 shows three typical bridging traction laws and their effects on notch sensitivity. A notable feature here is that the notch sensitivity is governed predominantly by the parameter α, and is relatively insensitive to the shape of the traction law. Moreover, for large values of $\alpha(\gtrsim 1)$, the notch-strength follows the Griffith relation [equation (1)], with $\Gamma = \Gamma_b$.

An additional feature that has been incorporated into recent calculations is the intrinsic fracture energy, Γ_0 [7, 8]. This energy can be represented by a non-dimensional parameter, λ, defined by

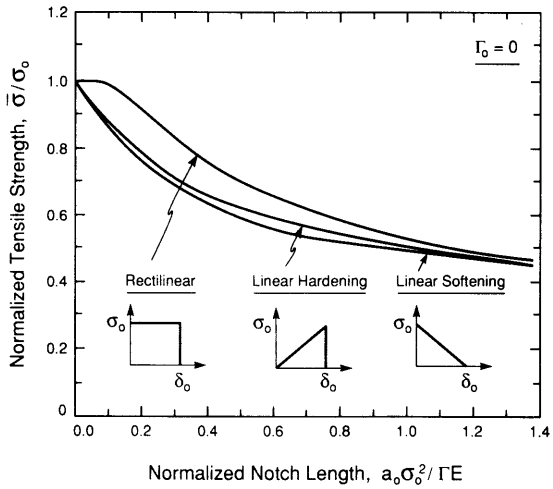

Fig. 1. Predicted trends in notch-strength with normalized notch size for several different forms of the bridging traction law.

$$\lambda = \Gamma_0/\Gamma_b. \tag{6}$$

Some trends in notch strength with λ for the rectilinear traction law are illustrated in Fig. 2. The main effect of λ is to increase the strength for small values of α. At higher values of α, the notch-strength again follows the Griffith relation, with Γ replaced by the total fracture energy: $\Gamma = \Gamma_0 + \Gamma_b$.

Calculations have also been performed to evaluate the strength of such materials in the presence of circular holes [7]. Figure 3 shows an illustrative example. For small values of α, the strength is similar to that corresponding to a sharp notch. However, for large values ($\alpha \gtrsim 1$) the strength asymptotically approaches the value predicted on the basis of the stress concentration factor, given by equation (3).

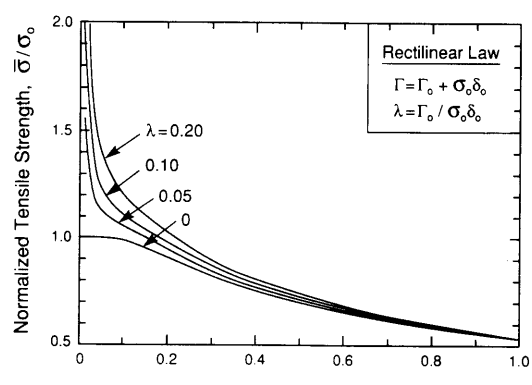

Fig. 2. Influence of the intrinsic toughness Γ_0 on the notch-strength characteristics for the rectilinear bridging traction law.

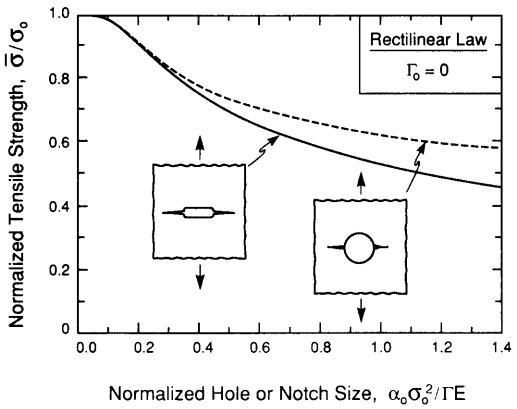

Fig. 3. Effects of circular holes vs sharp notches on strength.

3. EXPERIMENTS

3.1. Materials

The material used in this study was a Ti–6 Al–4 V matrix reinforced with unidirectional, continuous SiC fibers†, 100 μm in diameter. The composite panel was comprised of six plies, with a total thickness of 1.0 mm. The fiber volume fraction was 32%. Prior to consolidation, the fibers had been coated with ~ 1 μm of C, followed by ~ 1 μm of TiB_2. The TiB_2 coating serves as a diffusion barrier between the fiber and the matrix. During consolidation, the TiB_2 reacts with the matrix to form a layer of TiB needles, ~ 0.7 μm thick.

3.2. Tensile tests

Uniaxial tensile tests were conducted on specimens containing either notches or circular holes, located at the specimen center. To minimize damage, the specimens were prepared using electrical discharge machining (EDM). The holes ranged in length from 1.5 to 6 mm. The ratio of notch or hole size, $2a_0$, to specimen width, $2w$, was fixed at 0.2. In one case, where the hole size was 0.6 mm, specimens with a_0/w ratios of 0.2 and 0.05 were prepared and tested. In all cases, the ratio of specimen length to specimen width was greater than 3.

Prior to testing, one face of each specimen was polished to a 1 μm finish. Beveled stainless steel tabs were bonded to the specimen ends with an epoxy adhesive. In some instances, a 0.8 mm strain gauge was attached immediately ahead of the notch or hole. The tests were conducted in a servohydraulic testing machine, using hydraulic wedge grips to load the specimen. The tests were conducted at a fixed displacement rate, between 0.005 and 0.03 mm/min. For comparison, uniaxial tests were also conducted on straight (unnotched) tensile specimens, 6 mm wide, with axial strains measured using a 12.7 mm contacting extensometer. Additional details pertaining to the unnotched tensile strength of this material can be found in a companion paper [9].

†Sigma fiber, produced by British Petroleum.

3.3. Observations

During the tensile tests, the region immediately ahead of the notch or hole was monitored using a traveling stereo-microscope and recorded using a digital video camera. These observations were used to establish the extent of plasticity. In some cases, the tests were interrupted following the development of an extensive plastic zone (~ 1–3 mm), but prior to fracture. The extent of fiber fracture within this zone was determined by dissolving the matrix in the vicinity of the notch with a 49% HF solution and examining the underlying fibers in a scanning electron microscope (SEM). Some of the fracture surfaces were also examined in an SEM.

3.4. Toughness

The composite toughness, Γ, was evaluated using an edge-notched four-point work-of-rupture specimen [10, 11], shown in the inset of Fig. 9. (For reasons described below, the notched tensile tests could not be used to obtain Γ.) The test was conducted at a displacement rate of 0.5 mm/min. The toughness (or fracture energy) was evaluated using the relation

$$\Gamma = \frac{\int_0^{u_c} P \, du}{t(w - a_0)} \tag{7}$$

where P is the load, u is the load point displacement, u_c is the displacement at fracture, and t is the specimen thickness.

3.5. Bridging law parameters

As detailed in a subsequent section, the effects of holes and notches on the tensile strength of this composite can be rationalized in terms of crack bridging models. One of the important parameters involved in the bridging traction law is the crack opening displacement at fracture, δ_c. This parameter was determined in the notched specimens from measurements of the notch width both before and after fracture. The post-fracture notch width was taken to be the sum of the normal distances from the notch surfaces to the tips of the fracture surface, as shown in the inset of Fig. 10. Similar measurements were made on specimens with small holes (0.6 and 1.5 mm diameter).

Another key parameter in the traction law is the displacement δ_f at the onset of fiber failure. This displacement can be estimated using the relation

$$\delta_f \approx h_p \epsilon_f \tag{8}$$

where h_p is the width of the plastic zone measured parallel to the loading direction and ϵ_f is the failure strain of the fibers. The plastic zone size was measured off of micrographs of both sides of the fractured specimen, taken using Nomarski

interference microscopy. At each notch tip, ~20–30 such measurements were made, starting immediately ahead of the notch tip and proceeding at intervals of ~0.2 mm.

Yet another parameter in the traction law is the strength of the composite following fiber fracture. This strength was measured using a two-step procedure. First, a specimen with a 6 mm notch was loaded in tension until plastic strips ~3 mm long had developed on both sides of the notch. SEM examinations of similar specimens indicated that all the fibers had indeed fractured within this strip. Narrow, longitudinal strips (~2 mm wide), passing through the plastic strips, were then cut from the tested specimen. These strips were tested in tension, with a 10 mm clip gauge placed across the plastic strip to measure the local displacements.

4. EXPERIMENTAL RESULTS

Figures 4 and 5 show a typical stress–local strain response of a notched panel and a corresponding series of optical micrographs taken during the test. Initially, the response was linear, with non-linearity occurring at a stress of ~450 MPa. At a slightly higher stress (590 MPa), a plastic zone was observed at the notch tip [Fig. 5(a)]. Upon further loading, the length of the plastic strip increased stably, reaching ~3 mm at a stress of ~750 MPa. The specimen was subsequently unloaded for further examination. The local strain at the notch tip was ~5%: considerably higher than the fracture strain measured in the unnotched tensile specimens (~1%). The ultimate tensile strength of a similar specimen was ~850 MPa.

Examinations of specimens interrupted prior to fracture showed that *all* of the fibers contained within the plastic strips had been broken. Figure 6 shows one such example, from a specimen with a notch of length, $2a_0 = 3$ mm. In this case, both the plastic strip and the "plane" of fractured fibers follow the same,

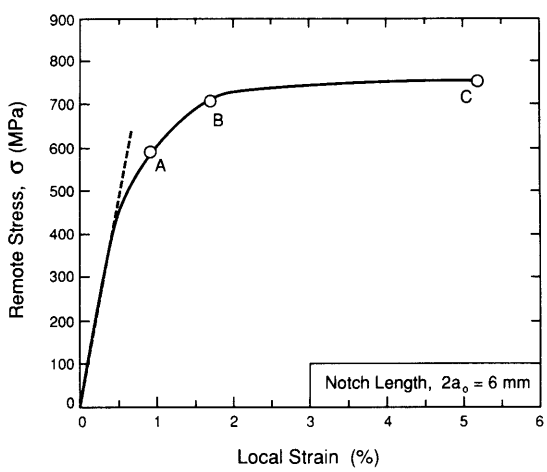

Fig. 4. The stress–local strain response of a specimen containing a 6 mm notch.

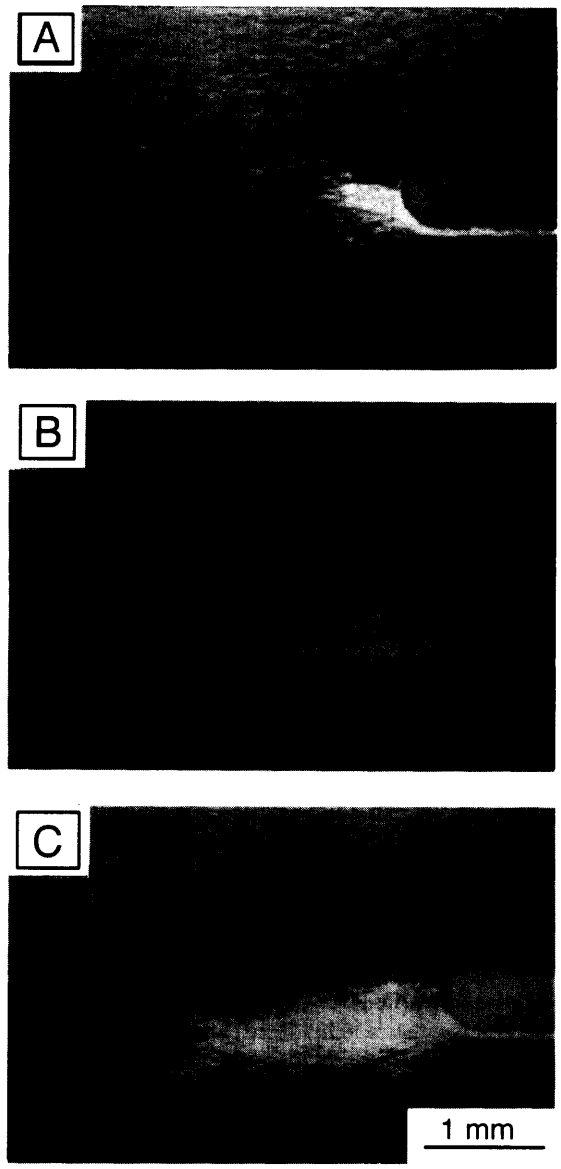

Fig. 5. Optical micrographs showing the progression of plastic strip development. The labels A, B, and C correspond to the stress levels shown in Fig. 4.

somewhat non-planar, path. The specimens containing circular holes exhibited similar patterns of plastic strips and fiber failure prior to catastrophic fracture.

Table 1. Summary of tensile test results

	Hole or notch size, $2a_0$ (mm)	Specimen width, $2W$ (mm)	Ratio, a_0/W	Ultimate tensile strength, σ_u (MPa)
Unnotched	—	6.0	—	1590 ± 100*
Hole	0.6	12.0	0.05	1210
Hole	0.6	3.0	0.20	1180
Hole	1.5	7.5	0.20	980
Hole	3.0	15.0	0.20	910
Hole	6.0	30.0	0.20	860
Notch	1.5	7.5	0.20	910
Notch	3.0	15.0	0.20	850
Notch	6.0	30.0	0.20	810

*Average and standard deviation from 8 tests.

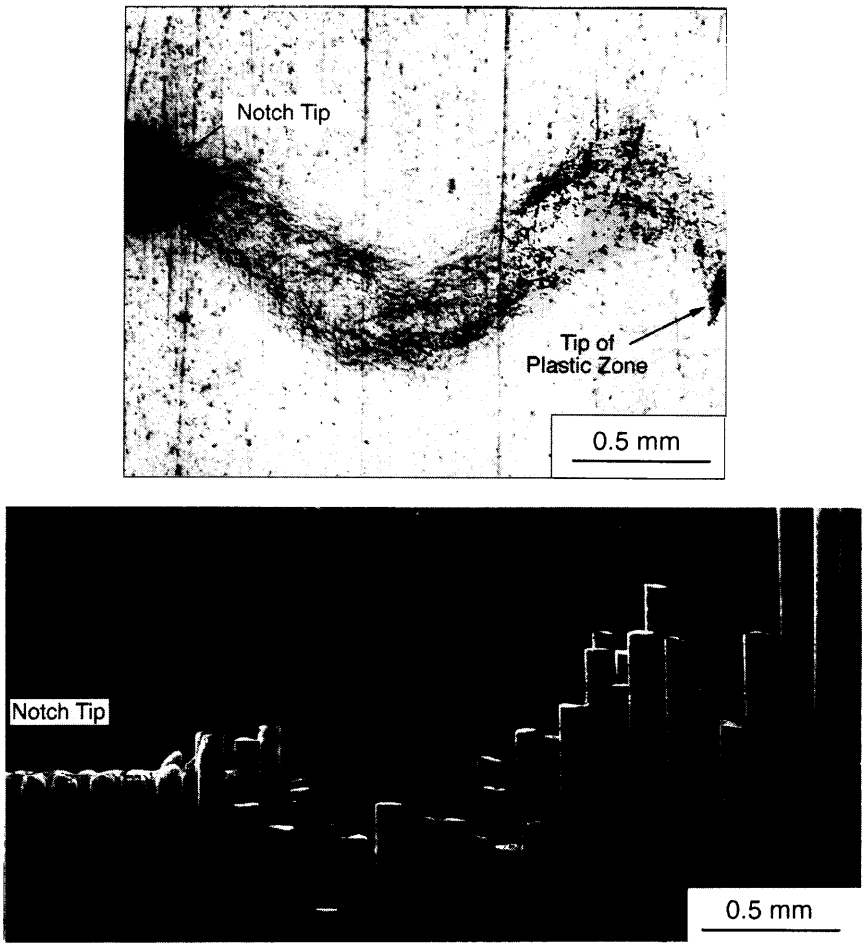

Fig. 6. Comparison of (a) the plastic strip ahead of a notch tip, with (b) the pattern of fiber fracture following matrix dissolution. The micrographs show identical regions of the specimen.

Fractographic examinations showed that minimal fiber pullout occurs during the fracture process (Fig. 7). The pullout length is typically $< 100\ \mu$m (i.e. one fiber diameter).

The trends in tensile strength $\bar{\sigma}$ with notch or hole size, $2a_0$, are summarized in Fig. 8. Evidently, the strength drops quickly with a_0 in the regime $0 < 2a_0 < 1.5$ mm. For larger values, $2a_0 \gtrsim 1.5$ mm, the strength continues to decrease, though at a much slower rate. The specimens containing holes exhibited similar trends, though the strengths were slightly higher than those corresponding to notches of the same size, by $\sim$6–7%.

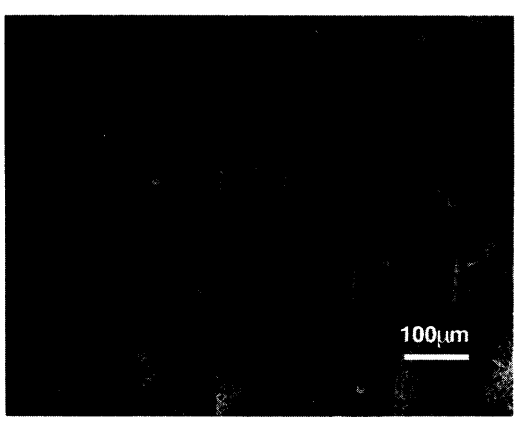

Fig. 7. SEM micrograph showing degree of fiber pullout.

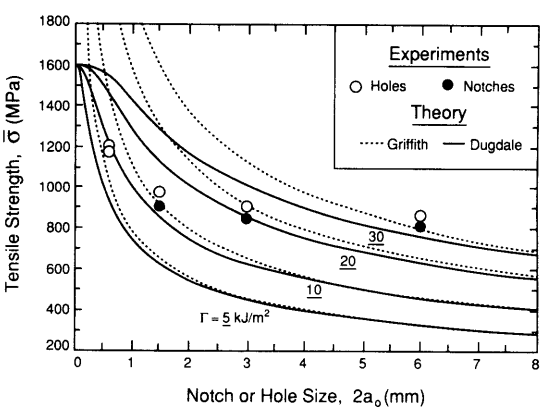

Fig. 8. Trends in tensile strength with hole or notch size. Also shown for comparison are predictions based on the Griffith equation and the Dugdale model.

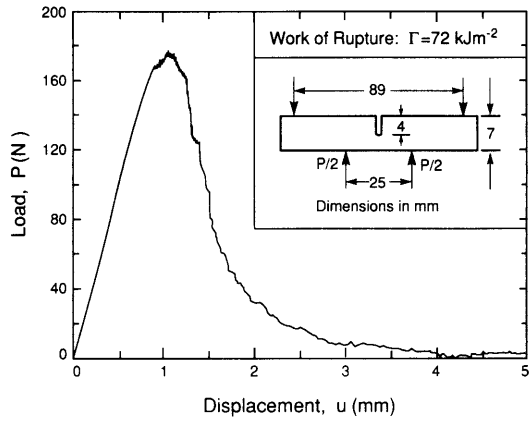

Fig. 9. Load–displacement curve measured on work-of-rupture specimen.

The results of the work of rupture test are shown in Fig. 9. Combining these measurements with equation (7) yields a toughness, $\Gamma = 72\ \mathrm{kJ\,m^{-2}}$. In this configuration, a similar process of plastic yielding was observed ahead of the notch tip. Once a crack had formed, it propagated stably across the specimen along a mode I path, resulting in a relatively smooth, continuous load–displacement curve.

The measurements of plastic zone width, h_p, and local displacement at fracture, δ_c, are summarized in Fig. 10. A typical optical micrograph used for measuring h_p and δ_c is shown in Fig. 11. The values of both parameters are independent of the specimen size and the specimen confirmation (notch vs hole), with average values, $h_p \approx 0.9$ mm and $\delta_c \approx 80\ \mu$m.

Figure 12 shows the results of a tensile test conducted on a specimen containing a plastic strip within which all fibers had been broken. The results are presented in the form of stress vs displacement (not strain), since virtually all the inelastic strain was localized within the previously yielded strip. In this test, the response was essentially elastic–perfectly plastic, with a "yield stress" of ~800–850 MPa (approximately one half of the unnotched tensile strength). The inelastic displacement at fracture was $\sim 40\ \mu$m. As expected, this value is lower than that measured on the notched tensile specimens (Fig. 10), a result of the prior inelastic deformation occurring during the development of the plastic strip.

5. ANALYSIS

5.1. Preliminary assessment

A preliminary assessment of the trends in notch strength was made using two simple modeling approaches. The first was based on the Griffith relation [equation (1)]. Figure 8 shows the predicted trends in strength with notch size for values of Γ ranging from 5 to 30 kJ m^{-2}. The second approach was based on the classical Dugdale model [equation (5)]. The predicted trends are also shown in Fig. 8, taking σ_0 to be equal to the unnotched tensile strength ($\bar{\sigma}_0 = 1590$ MPa) and Γ to range between 5 and 30 kJ m^{-2}, as before. It is apparent that neither approach provides even a fair representation of the experimental measurements. This disparity between experiment and theory provides the motivation for the subsequent modeling effort. Moreover, it demonstrates that the trends in tensile strength with notch length cannot be used to infer the composite toughness.

5.2. Proposed bridging traction law

The present measurements and observations suggest that the notch strength characteristics of the Ti/SiC composite can be rationalized in terms of a bridging traction law having the features shown on Fig. 13. In this law, the stress initially increases with displacement, analogous to the stress–strain response measured in a uniaxial tension test. At a critical stress, S_1, taken to be the unnotched tensile strength of the composite, $\bar{\sigma}_0$, the fiber bundle within the bridging zone fails, causing the stress to drop rather precipitously with increasing crack opening displacement. The corresponding critical displacement, δ_1,

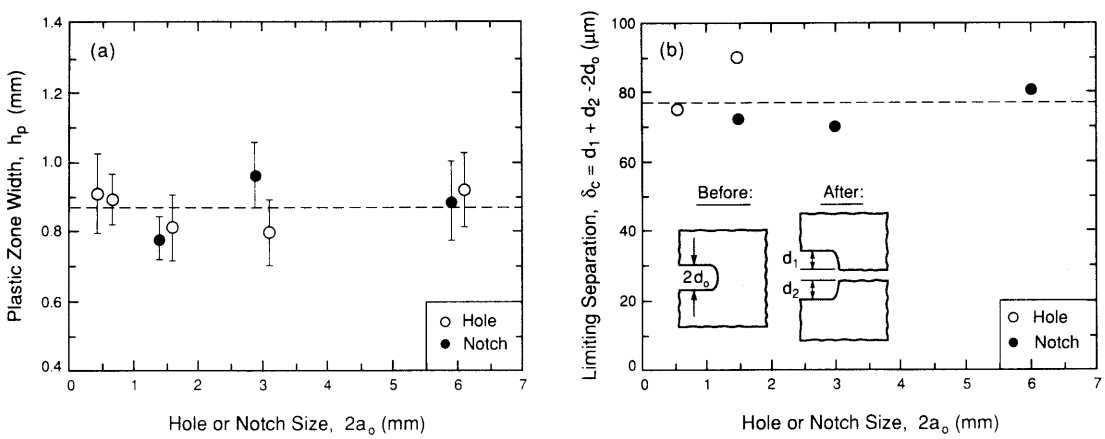

Fig. 10. Trends in (a) plastic zone width, h_p, and (b) local displacement at fracture, δ_c, with hole or notch size.

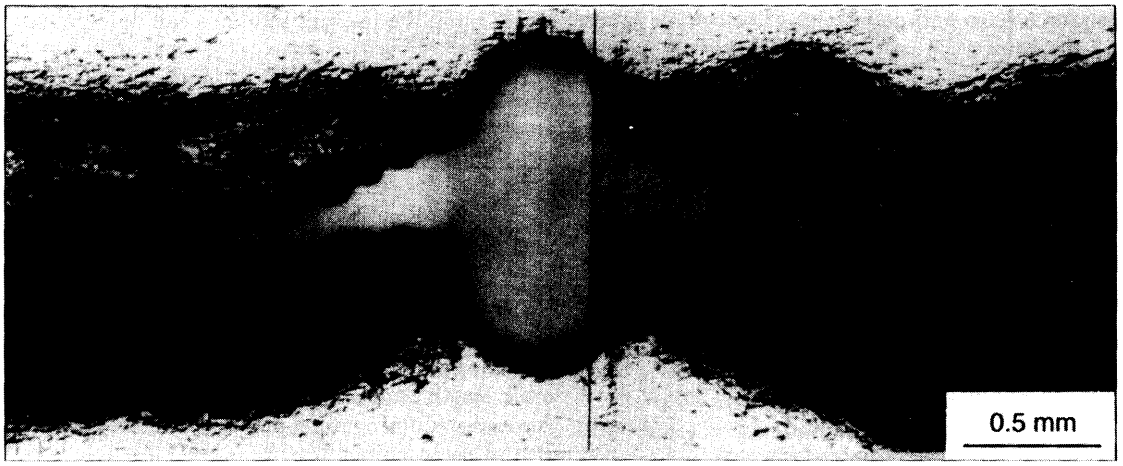

Fig. 11. Optical micrograph showing plasticity around the hole following fracture.

depends on the width of the plastic strip (being the effective gauge length) and the fiber failure strain, in accordance with equation (8). Upon further crack opening, the bridging stress reaches a saturation level, dictated by the yield stress of the metal and the "pullout" contribution from broken fibers (detailed later). At a yet larger crack opening displacement, the local strain reaches the failure strain of the metal, leading to the formation of a matrix crack and a loss in bridging.

For modeling purposes, it is convenient to represent this behavior by a two level bridging traction law, shown schematically by the dashed lines in Fig. 13. Each of the two parts of the traction law are characterized by a strength (S_1 or S_2) and a critical displacement (δ_1 or δ_2). The total (or steady state) fracture energy, obtained using the J-integral, is

$$\Gamma = \int_0^{\delta_2} \sigma_b \, d\,\delta = \Gamma_1 + \Gamma_2 \tag{9a}$$

where Γ_1 and Γ_2 are the areas contained within the top and bottom parts of the traction law, given by

$$\Gamma_1 = (S_1 - S_2)\,\delta_1 \tag{9b}$$

and

$$\Gamma_2 = S_2\,\delta_2. \tag{9c}$$

A preliminary assessment of the proposed traction law can be made by comparing the total fracture energy, computed using equation (9) along with the measured values of the traction law parameters, with the value obtained through the work-of-rupture test. The experimental measurements indicate that $S_1 = \bar{\sigma}_0 = 1590$ MPa, $S_2 = 850$ MPa (Fig. 12), and $\delta_2 = 80\ \mu$m. Moreover, combining the plastic zone width, $h_p = 0.9$ mm, and the unnotched tensile fracture strain, $\epsilon_f = 1\%$, with equation (8) yields $\delta_1 \approx 9\ \mu$m. Equation (9) thus predicts a fracture energy, $\Gamma = 71$ kJ m^{-2}, essentially identical to the value obtained experimentally ($\Gamma = 72$ kJ m^{-2}). This correlation provides some initial confidence in the proposed traction law.

5.3. *Model of notch strength*

For the purpose of modeling the notch-strength behavior of such a material, the two-level rectilinear

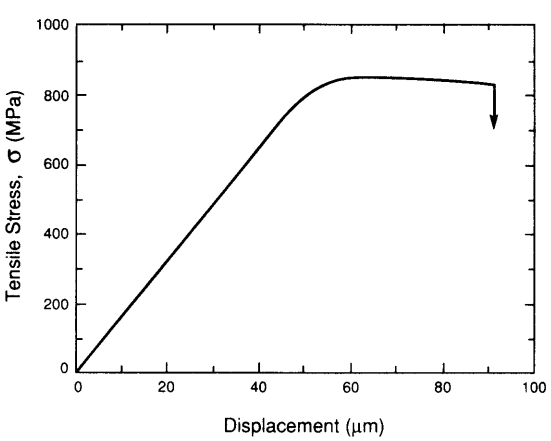

Fig. 12. Tensile test of specimen containing plastic strip with broken fibers.

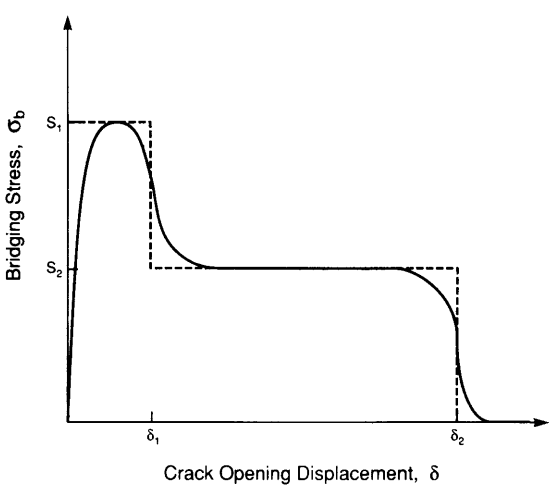

Fig. 13. Schematic diagram of the proposed traction law governing fracture in the Ti/SiC composite.

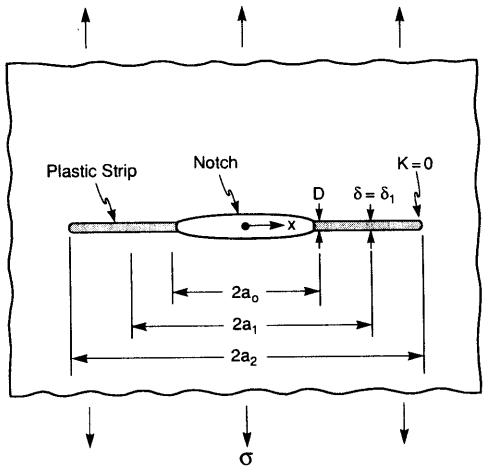

Fig. 14. Schematic diagram of the crack bridging model.

law was incorporated into a fracture mechanics model, shown schematically in Fig. 14. In the model, the composite panel is taken to be infinitely large and contain a sharp, through-thickness notch of length, $2a_0$. The panel is loaded remotely with a uniform tensile stress, σ. The material is assumed to be linearly elastic, except within the plastic strips formed ahead of the notch tips. The stress intensity factor K at the tip of the plastic zone is taken to be zero, such that the material possesses no intrinsic toughness. Two relevant "crack lengths" are identified. The first, $2a_1$, represents the point at which the crack opening displacement δ reaches the critical value, δ_1. Ahead of this point, the tractions on the crack face are given by S_1, and behind it, by S_2. The total crack length (notch and plastic strip) is designated $2a_2$, and the crack opening displacement at the notch tip is designated D.

Two regimes are considered, goverened by the value of D. In the first, $D < \delta_1$, such that the model reduces to the classical Dugdale–Barenblatt model, with a uniform bridging stress, S_1. The plastic strip thus extends according to [3, 4]

$$\frac{\sigma}{S_1} = \frac{2}{\pi}\cos^{-1}\left(\frac{a_0}{a_2}\right) \tag{10}$$

with a crack opening displacement at the notch tip of

$$\frac{DE}{a_0 S_1} = \frac{8}{\pi}\ln\frac{a_2}{a_0}. \tag{11}$$

The maximum stress is obtained by combining equations (10) and (11) and setting $D = \delta_1$. In the second regime, D lies in the range $\delta_1 < D < \delta_2$, such that the plastic zone consists of two parts. Along the part of the crack plane defined by $a_0 < |x| < a_1$, the bridging stress is S_2, and, in that part defined by $a_1 < |x| < a_2$, the bridging stress is S_1, as noted ear lier. The stress-crack length relations are obtained from handbook solutions of stress intensity factors and crack opening displacements [13]. In non-dimensional form, the relevant solutions can be expressed as

$$\frac{\delta_1 E}{\sigma a_0} = f_1 - f_2\frac{S_1}{\sigma} - f_3\frac{S_2}{\sigma} \tag{12}$$

$$\frac{K}{\sigma\sqrt{\pi a_0}} = g_1 - g_2\frac{S_1}{\sigma} - g_3\frac{S_2}{\sigma} \tag{13}$$

and

$$\frac{DE}{\sigma a_0} = h_1 - h_2\frac{S_1}{\sigma} - h_3\frac{S_2}{\sigma} \tag{14}$$

where the parameters f_i, g_i and h_i are functions of the crack length ratios, a_1/a_0 and a_2/a_0, and are listed in Appendix A. Recognizing that $K = 0$ allows equation (13) to be re-written as

$$\frac{\sigma}{S_1} = \frac{g_2}{g_1} + \frac{g_3}{g_1}\frac{S_2}{S_1} \tag{15}$$

which, combined with equation (12), gives

$$\frac{\delta_1 E}{S_1 a_0} = \left(\frac{g_2}{g_1} + \frac{g_3 S_2}{g_1 S_1}\right) f_1 - f_2 - f_3\frac{S_2}{S_1}. \tag{16}$$

The stress–crack opening displacement curve is obtained by incrementally stepping through values of a_1/a_0, starting with the one evaluated using equation (11) with $D = \delta_1$. At each point, the ratio a_2/a_0 is evaluated by numerically solving equation (16) and the result then combined with equations (12) and (14) to get σ and D, respectively.

Figure 15 shows illustrative examples of the trends in σ with D for a strength ratio, $S_1/S_2 = 2$, and a toughness ratio, $\Gamma_1/\Gamma_2 = 0.1$. For reasons that will become apparent in the subsequent section, the toughness ratio Γ_1/Γ_2 is designated λ, analogous to equation (6). Three types of behavior are obtained, governed by the normalized notch length, α. (i) For very small notch lengths ($\alpha \ll 1$), the maximum stress is reached almost immediately after D exceeds δ_1. In this case, the ductility of the matrix (manifested in the critical displacement, δ_2) does not increase the notch

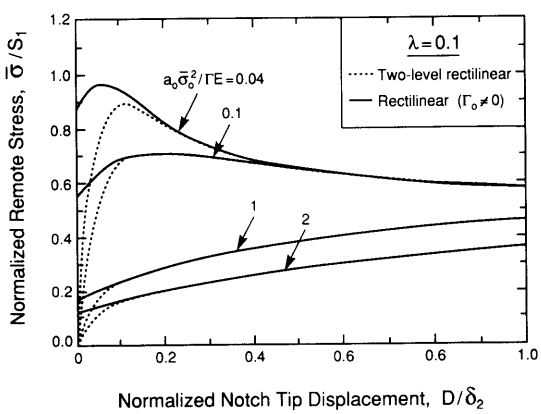

Fig. 15. Predicted stress–crack opening curves for the two traction laws: (i) the two-level rectilinear law, with no intrinsic toughness ($\Gamma_0 = 0$), and (ii) the rectilinear law, with an intrinsic toughness, Γ_0.

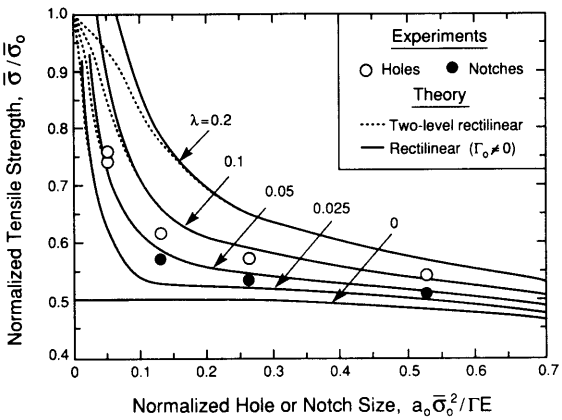

Fig. 16. Comparisons between experimental measurements and predictions of models based on (i) the two-level rectilinear traction law, (ii) and the simple rectilinear law, with an intrinsic toughness Γ_0.

strength of the composite. (ii) For intermediate sized notches, the maximum stress occurs at a value of D that is substantially larger than δ_1. Consequently, composite fracture does not occur immediately following the onset of fiber failure. Here, the matrix ductility provides some enhancement in tensile strength. (iii) For very long notches ($\alpha \gg 1$), the maximum stress is obtained when the matrix fails, i.e. $D = \delta_2$. The relationship between strength, $\bar{\sigma}$, and notch length, α, is obtained from the maximum points in these curves.

Figure 16 shows the predicted trends in strength with notch length, for $S_1/S_2 = 2$ and Γ_1/Γ_2 ranging from 0 to 0.2. Also shown are the values obtained experimentally. The comparisons show that the predictions are in close agreement with the measurements for Γ_1/Γ_2 in the range $\sim$0.03–0.1. The inferred value of Γ_1/Γ_2 is comparable to the one calculated using the values of S_1, S_2, δ_1 and δ_2 quoted above: $\Gamma_1/\Gamma_2 \sim 0.09$.

Because of the similarities in the strength characteristics of the specimen containing holes and notches, no calculations were conducted for holes. The similarities are consistent with previous calculations which show that the strength of materials that exhibit bridging is insensitive to the shape of the discontinuity, provided the bridging length scale is sufficiently large compared with a_0. Indeed, for the entire range of hole and notch sizes used in this study, the normalized notch size lies in the range $\alpha \lesssim 0.5$ (Fig. 3).

5.4. An alternate approach

It is instructive to consider an alternate description of the fracture resistance: one that leads to a simpler solution to the notch sensitivity. For this purpose, it is noted that the energy dissipated in the top portion of the traction law is small in relations to the total. (i.e. $\Gamma_1/\Gamma_2 \sim 0.05$). Moreover, the critical displacement δ_1 is small in relation to δ_2. Consequently, the energy dissipated in the top portion can be lumped into an *intrinsic* fracture energy, Γ_0, whereupon

$$\Gamma_0 = \Gamma_1 = (S_1 - S_2)\,\delta. \tag{17}$$

The fracture resistance can thus be characterized by Γ_0 in combination with a single-level rectilinear bridging traction law, with a characteristic strength, S_2, and a critical displacement, δ_2. The toughness derived from bridging is thus

$$\Gamma_b \equiv \Gamma_2 = S_2\,\delta_2 \tag{18}$$

and the toughness ratio is again defined by $\lambda = \Gamma_0/\Gamma_b$.

The notch strength of such a system can be evaluated following the approach presented in the preceding section, with two modifications. First, since the stress along the entire bridged zone is uniform, a_1 is equivalent to a_0. Second, the crack tip stress intensity factor is finite and taken to be equal to the intrinsic fracture toughness, $\sqrt{\Gamma_0 E}$. In this case, equations (12)–(14) reduce to

$$\sqrt{\frac{\Gamma_0 E}{\sigma^2 \pi a_0}} = \sqrt{\frac{a_2}{a_0}} - \frac{2}{\pi}\sqrt{\frac{a_2}{a_0}}\frac{S_2}{\sigma}\cos^{-1}\left(\frac{a_0}{a_2}\right) \tag{19}$$

and

$$\frac{DE}{\sigma a_0} = 4\sqrt{\left(\frac{a_2}{a_0}\right)^2 - 1} - \frac{8}{\pi}\frac{S_2}{\sigma} \times \left(\sqrt{\left(\frac{a_2}{a_0}\right)^2 - 1}\cos^{-1}\left(\frac{a_0}{a_2}\right) - \ln\frac{a_2}{a_0}\right). \tag{20}$$

The stress–crack opening relation is obtained by incrementally stepping through values of a_2/a_0, starting from zero. At each point, the stress σ is evaluated from equation (19) and the result combined with equation (20) to obtain D. Figure 15 shows comparisons of the predicted trends in σ vs D with those obtained from the two-level rectilinear law. Evidently, the two solutions provide essentially the same results for $D/\delta_2 \gtrsim 0.1$.

Figure 16 shows the predicted trends in strength with notch length, again for values of λ ranging from 0 to 0.2. Over the range of interest ($\alpha \gtrsim 0.1$, $\lambda \lesssim 0.1$), the predictions are essentially identical to those of the two-level bridging law. For smaller values of α, the model predicts a strength-notch length relation of the form

$$\frac{\bar{\sigma}}{S_1} = \sqrt{\frac{E\Gamma_0}{\pi a_0 S_1^2}} \tag{21}$$

in accordance with the Griffith equation. In this regime, the model strongly overestimates the notch-strength of the composite. Consequently, the two-level bridging law is required to capture the relevant trends.

It is of interest to note, parenthetically, that a conservative estimate of the notch strength can be obtained by assuming $\lambda = 0$, whereupon both models reduce to the Dugdale–Barenblatt model [equation (5)], with the bridging stress replaced by $S_2 = S_1/2$.

6. DISCUSSION

The present measurements allow some rudimentary connections to be established between the parameters involved in the traction law and the properties of the composite constituents. Such connections are important in understanding the role of microstructure in composite behavior and provide guidance for the development of new materials.

As noted previously, the peak stress, S_1, is equivalent to the unnotched composite tensile strength, $\bar{\sigma}_0$. This strength is controlled by the matrix yield stress and the *in situ* fiber bundle strength, as described in a companion paper [9]. For this class of composite, the fiber bundle strength is *independent* of gauge length, provided the gauge length exceeds a critical value

$$l_c = \left(\frac{S_0 R L_0^{1/m}}{\tau}\right)^{m/(m+1)} \tag{22}$$

where τ is the interfacial sliding stress, R is the fiber radius, S_0 is the reference strength corresponding to a length L_0 in the Weibull distribution, and m is the Weibull modulus. In the Ti/SiC composite, the critical length is of the order, $l_c \approx 2$ mm: being approximately twice the relevant gauge length in the bridging process, namely, the plastic zone width, h_p. Simulations of fiber bundle failure for gauge lengths in the range $0.5 < l/l_c < 1$ suggest that the tensile strength is elevated only slightly ($\sim$5–10%) over the value corresponding to a long gauge length ($l/l_c \geq 1$)[12]. Consequently, S_1, is expected to be essentially the same as the tensile strength measured on a standard tensile coupon.

Bounds on the strength, S_2, characterizing the post-fiber failure regime, can be established in the following way. An upper bound estimate is obtained by taking the average stress acting across a hypothetical crack plane passing through the middle of the plastic zone, whereupon

$$S_2 = (1-f)\sigma_m^y + f\hat{\sigma}_f \tag{23}$$

with $\hat{\sigma}_f$ being the average fiber stress resulting from fiber/matrix sliding following fiber fracture. For simplicity, the fiber failure sites are assumed to be randomly distributed within the plastic zone, with an average distance between the fracture sites and the hypothetical plane of $\sim h_p/4$ (Fig. 17). Using a simple shear lag model, $\hat{\sigma}_f$ can be approximated by

$$\hat{\sigma}_f \approx \tau h_p / 2R. \tag{24}$$

Using the relevant measurements ($h_p \approx 800\,\mu$m, $R = 50\,\mu$m, $\tau = 130$ MPa, $\sigma_m^y = 1000$ MPa) yields a value of strength, $S_2 \approx 1000$ MPa, somewhat higher than the measured value (850 MPa). This discrepancy may be attributed to the pullout distances being less than $h_p/4$ ($\sim 200\,\mu$m), as manifest in the relatively short pullout lengths measured on the fracture surface ($< 100\,\mu$m). A lower bound estimate is obtained by neglecting the pullout contribution derived from broken fibers, whereupon the strength reduces to

$$S_2 = (1-f)\sigma_m^y. \tag{25}$$

This result predicts a value of strength, $S_2 \approx 680$ MPa, somewhat lower than the measured value.

The critical displacements, δ_1 and δ_2, are both expected to scale with the width of the plastic zone. As noted earlier, δ_1 is governed by the strain at fiber bundle failure, in accordance with equation (8). Similarly, δ_2 scales with the ductility of the matrix, $\bar{\epsilon}_m$, according to the relation

$$\delta_2 \approx \bar{\epsilon}_m h_p. \tag{26}$$

Combining the measured values, $\delta_2 \approx 80\,\mu$m and $h_p \approx 0.9$ mm, with equation (26) yields an estimate of the matrix ductility, $\bar{\epsilon}_m \approx 9\%$, in agreement with values reported for similar Ti alloys [8–10%] [14].

The origin of the plastic zone width is presently not understood. It is speculated that it may be controlled by the panel thickness (≈ 1 mm), as it is in thin ductile sheets [2]. This hypothesis requires experimental verification.

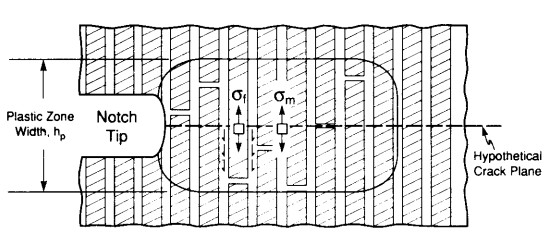

Fig. 17. Schematic diagram showing contribution from matrix yielding and fiber pullout on the composite strength in the post-fiber failure regime.

7. CONCLUDING REMARKS

The present study demonstrates that the notch-strength characteristics of fiber-reinforced Ti matrix composites can be described using crack bridging models, similar to those used to describe the behavior of ductile metals and ceramic matrix composites. The parameters controlling the bridging traction law have been measured and found to provide a consistent description of both the notch sensitivity and the steady state composite toughness. The two models considered here (one based on the two-level rectilinear bridging law and the other on the rectilinear law with a finite intrinsic toughness) yield similar predictions for notch sizes that are relevant in structural design ($2a_0 \geq 1$ mm). Owing to its simplicity, the latter model is preferred. The models are computationally relatively simple, making them amenable for use in design.

Acknowledgement—Funding for this work was supplied by the DARPA University Research Initiative Program at UCSB under ONR contract N0014-92-J-1808.

REFERENCES

1. J. Doychak, *J. Metals* **44,** 46 (1992).
2. D. S. Dugdale, *J. appl. Mech.* **8,** 100 (1960).
3. B. A. Bilby, A. H. Cottrell and K. H. Swindon, *Proc. Soc. Lond. A* **272,** 304 (1963).
4. A. H. Cottrell, *Tewksbury Symp. on Fracture*. Univ. of Melbourne Press (1963).
5. J. R. Rice, *J. appl. mech.* **35,** 379 (1968).
6. D. B. Marshall and B. N. Cox, *Acta metall.* **35,** 2607 (1987).
7. Z. Suo, S. Ho and X. Gong, *J. Engng Mater. Technol.* **115,** 319 (1993).
8. G. Bao and F. Zok, *Acta metall. mater.* **41,** 3515 (1993).
9. C. H. Weber, X. Chen, S. J. Connell and F. W. Zok, *Acta metall. mater.* **42,** 3443 (1994).
10. H. G. Tattersall and G. Tappin, *J. Mater. Sci.* **1,** 296 (1966).
11. J. I. Bluhm, *Engng Fract. Mech.* **7,** 593 (1975).
12. F. Hild, J. M. Domergue, F. A. Leckie and A. G. Evans, *Int. J. Solids Struct.* **31,** 1035 (1994).
13. H. Tada, P. C. Paris and C. R. Irwin, *The Stress Analysis of Cracks Handbook*, 2nd edn. Paris Productions Inc., St. Louis, Miss. (1985).
14. *Metals handbook*, 9th edn, Vol. 3, pp. 388–391. ASM, Metals Park, Ohio, (1990).

APPENDIX A

The geometric parameters, f_i, g_i and h_i, in equations (12)–(14) are given by [13]

$$f_1 = 4\sqrt{\eta_2^2 - \eta_1^2} \tag{A1}$$

$$f_2 = \frac{8}{\pi}\left[\sqrt{\eta_2^2 - \eta_1^2}\cos^{-1}\left(\frac{\eta_1}{\eta_2}\right) - \eta_1 \ln\left(\frac{\eta_2}{\eta_1}\right)\right] \tag{A2}$$

$$f_3 = \frac{8}{\pi}\left\{\sqrt{\eta_2^2 - \eta_1^2}\left[\sin^{-1}\left(\frac{\eta_1}{\eta_2}\right) - \sin^{-1}\left(\frac{1}{\eta_2}\right)\right] + \eta_1 \ln\left(\frac{\eta_2}{\eta_1}\right)\right\} + \frac{8}{\pi}\left\{\eta_1 \tanh^{-1}\sqrt{\frac{(\eta_2/\eta_1)^2 - 1}{\eta_2^2 - 1}} - \tanh^{-1}\sqrt{\frac{\eta_2^2 - \eta_1^2}{\eta_2^2 - 1}}\right\} \tag{A3}$$

$$h_1 = 4\sqrt{\eta_2^2 - 1} \tag{A4}$$

$$h_2 = \frac{8}{\pi}\left[\sqrt{\eta_2^2 - 1}\cos^{-1}\left(\frac{\eta_1}{\eta_2}\right)\right] + \frac{8}{\pi}\left[\coth^{-1}\sqrt{\frac{\eta_2^2 - 1}{(\eta_2/\eta_1)^2 - 1}} - \eta_1 \coth^{-1}\sqrt{\frac{\eta_2^2 - 1}{\eta_2^2 - \eta_1^2}}\right] \tag{A5}$$

$$h_3 = -\frac{8}{\pi}\left\{\sqrt{\eta_2^2 - 1}\left[\sin^{-1}\left(\frac{1}{\eta_2}\right) - \sin^{-1}\left(\frac{\eta_1}{\eta_2}\right)\right] + \ln \eta_2\right\} + \frac{8}{\pi}\left\{-\coth^{-1}\sqrt{\frac{\eta_2^2 - 1}{(\eta_2/\eta_1)^2 - 1}} + \eta_1 \coth^{-1}\sqrt{\frac{\eta_2^2 - 1}{\eta_2^2 - \eta_1^2}}\right\} \tag{A6}$$

$$g_1 = \sqrt{\eta_2} \tag{A7}$$

$$g_2 = \frac{2}{\pi}\sqrt{\eta_2}\cos^{-1}\left(\frac{\eta_1}{\eta_2}\right) \tag{A8}$$

$$g_3 = \frac{2}{\pi}\sqrt{\eta_2}\left[\cos^{-1}\left(\frac{1}{\eta_2}\right) - \cos^{-1}\left(\frac{\eta_1}{\eta_2}\right)\right] \tag{A9}$$

where η_1 and η_2 are normalized crack lengths defined by

$$\eta_1 \equiv a_1/a_0 \tag{A10}$$

and

$$\eta_2 \equiv a_2/a_0. \tag{A11}$$

APPENDIX B

Nomenclature

$2a_0$	notch width, or hole diameter
$2a_1$	crack length at $\delta = \delta_1$
$2a_2$	total length of notch and plastic strip
c	flaw size
D	crack opening displacement at notch tip
E	Young's modulus
f_i, g_i, h_i	geometric parameters (Appendix A)
h_p	plastic zone width
K	crack tip stress intensity factor
l_c	critical (transfer) length
L_0	reference length (1 m)
m	Weibull modulus
P	load
R	fiber radius
S_0	reference strength, corresponding to $L_0 = 1$ m
S_1, S_2	bridging stresses in two-level rectilinear law
t	panel thickness
w	half width (width for edge notched specimen)
α	normalized notch length ($a_0\,\bar{\sigma}_0^2/\Gamma E$)
δ	crack opening displacement (COD)
δ_1, δ_2	critical values of δ in bridging traction law
δ_f	COD needed for fiber fracture
δ_c	COD needed for matrix fracture
ϵ_f	fiber failure strain
ϵ_m	matrix failure strain
Γ	fracture energy
Γ_1, Γ_2	components of fracture energies from bridging
Γ_b	fracture energy derived from bridging
Γ_0	intrinsic toughness
λ	toughness ratio ($\lambda = \Gamma_0/\Gamma_b$ for rectilinear law, $\lambda = \Gamma_1/\Gamma_2$ for two-level rectilinear law)
σ	remote tensile stress
σ_0	bridging stress
$\bar{\sigma}$	notched tensile strength
$\bar{\sigma}_0$	unnotched tensile strength
σ_m^y	matrix yield stress
σ_y	yield stress of monolithic metal
τ	interfacial sliding stress